Hong, John, Jang, A-Rang, Park, Woon Bae, Hou, Bo , Lee, Jeong-O, Sohn, Kee-Sun, Cha, SeungNam, Lee, Young-Woo and Sohn, Jung Inn 2021. Thermodynamically and physically stable dendrite-free Li interface with layered boron nitride separators. ACS Sustainable Chemistry and Engineering 9 (11) , pp. 4185-4193. 10.1021/acssuschemeng.1c00040

Publishers page: http://dx.doi.org/10.1021/acssuschemeng.1c00040

Thermodynamically and Physically Stable Dendrite-Free Li Interface with Layered Boron Nitride Separators

John Hong[a,b,†], A-Rang Jang[c,†], Woon Bae Park[d], Bo Hou[e], Jeong-O Lee[f], Kee-Sun Sohn[g], SeungNam Cha[h], Young-Woo Lee[i,*] and Jung Inn Sohn[j,*]

[a] Energy Storage & Distributed Resources Division, Lawrence Berkeley National Laboratory, 1 Cyclotron Rd, Berkeley, CA 94720, USA

[b] School of Materials Science and Engineering, Kookmin University, 77 Jeongneung-Ro, Seoul 02707, Republic of Korea

[c] Department of Electrical Engineering, Semyung University, 65 Semyung-ro, Chungcheongbuk-do 27136, Republic of Korea

[d] Department of Printed Electronics, Sunchon National University, 291-19 Jungang-ro, Sunchon, Jeollanam-do 57922, Republic of Korea

[e] Department of Physics and Astronomy, Cardiff University, 5 The Parade, Newport Road, Cardiff CF24 3AA, United Kingdom

[f] Advanced Materials Division, Korea Research Institute of Chemical Technology (KRICT), 141 Gajeong-Ro, Daejeon 34114, South Korea

[g] Department of Nanotechnology and Advanced Materials Engineering, Sejong University, 39 Sejong-Daero Seoul 05006, Republic of Korea

[h] Department of Physics, Sungkyunkwan University (SKKU), 2066 Seobu-Ro, Suwon, Gyeonggi-Do 16419, Republic of Korea

[i] Department of Energy Systems, Soonchunhyang University, 2 Soonchunhyang-Ro, Asan, Chungcheongnam-Do 31538, Republic of Korea

[j] Division of Physics and Semiconductor Science, Dongguk University-Seoul, 30 Pildong-Ro Seoul 04620, Republic of Korea

Corresponding Author (Prof. Young-Woo Lee and Prof. Jung Inn Sohn)

E-mail address: ywlee@sch.ac.kr, junginn.sohn@dongguk.edu

[†] Those authors contributed equally to this work.

Abstract

The development of promising separator candidates, offering both great physical rigidity and high thermal resistance, is still a global challenge to guarantee high-performance electrochemical cells. Freestanding hexagonal boron nitride (*h*-BN) separators are developed using the strategically combined synthetic steps with liquid and thermal-expansion exfoliation methods, which can simply fabricate the largely yielded *h*-BN nanosheets. The as-prepared freestanding *h*-BN nanosheet separator presents the better ionic conductivity than commercial polymer separators, and furtherly provides the excellent stability of Li-ion cells by suppressing the protruding dendritic Li growth during cycles on the electrodes as well as the high thermal and electrochemical stability of *h*-BN nanosheet separators even after aging process at high temperature 80~120 °C. Furthermore, the lithium titanate (LTO) batteries with the freestanding *h*-BN separators maintain an outstanding reversible coulombic efficiency of ~ 99 % after 600 cycles as well as high cycling retention, indicating the significant improvement on battery performance compared to the LTO batteries with commercial polymer separators. Thus, the freestanding *h*-BN separators may provide a new strategic way for the efficient storage of charge in next-generation rechargeable batteries and high-safety energy storage applications.

Keywords: hexagonal boron nitride, two-dimensional atomic crystal, layered separator, thermal stability, lithium metal anode

Introduction

Currently, to meet the ever-increasing demands of electrical energy delivery, electrochemical lithium ion batteries (LIBs) are a primary class of energy storage and delivery sources in portable electronic applications [1-4]. Particularly, in order to optimize and further improve the overall energy-storing performance of LIBs, the rational selection and design of each conventional battery component (such as electrodes, electrolyte, and separators) are very essential [5-7]. In fact, many studies on LIBs have intensively focused on the improvement of energy storage capacitance and cyclability by the optimization of electrode and electrolyte materials [8-9]. However, there are more crucial factors which may limit the overall performance of LIBs such as the growth of protruding Li dendrites during cycling and the physical and chemical damage through internal and external heat environments [10-11]. Such factors can induce the serious deformation of separator membranes and cause drastic performance failure as well as severe problems on battery safety [12]. Commercial separators are largely consisted of polymer-based compounds, which can be certainly damaged by the aforementioned factors during cycling. Therefore, the development of novel separators with high electrochemical, physical, and thermal stability is important not only for viable long-term and high-performance LIB applications but also for the use of Li metal as the anode, possessing a high theoretical specific capacity of 3860 mAh g^{-1} and a low redox potential (-3.04 V vs. standard hydrogen electrode) [13-17]. Recently, to suppress Li dendrite growth, the deposition of some nanomaterials (such as silicone nanofilaments, dopamine and mesoporous silica thin films) on commercial separators has been reported and presented the high electrochemical stability [15-16]. Moreover, the coated Prussian blue and reduced graphite oxides on commercial separator also show the ultra-long-term stability of Li plating/stripping [17]. However, instead of focusing on new coating materials on commercial separators, the development of freestanding materials candidates for separators may be a crucial way to solve Li dendrite problems which are usually originated from polymer-based commercial separators.

Hexagonal boron nitride (h-BN), as a typical two-dimensional (2D) insulating material with a wide band gap (5-6 eV), has been considered to be a promising candidate for separator membranes in LIBs because of its outstanding ion permeability as well as superior thermal, chemical and physical stability [18-20]. h-BN films have recently revealed great success as stable coating materials on electrodes and polymer membranes, which can lead to the great strides in increasing the performance and stability of LIBs. For example, Yan et al. and Xie et al. reported that the 2D h-BN layers were directly synthesized on a Cu foil using a chemical vapor deposition (CVD) method [21-22]. The 2D h-BN layers can effectively suppress the growth of Li dendrites and hence, improve the cycling stability. Furthermore, Kim et al. and Luo et al. reported that the commercial polymer separators coated with the h-BN materials can improve the coulombic efficiency and ensure the reliability of Li metal anodes [23-24]. Nevertheless, the CVD-grown h-BN films are not practical to utilize as commercial and practical products due to its low reproducibility and limitation of large-scale fabrication. Indeed, the h-BN coated commercial polymer separators can be also damaged by any internal or external heat sources, resulting in the issues of dramatic performance degradation or safety failure. Therefore, it is highly desirable to fabricate freestanding h-BN separators, which are made of h-BN itself from new practical and scalable synthetic routes.

In this work, freestanding h-BN nanosheet (BNN) separators represent the outstanding thermal endurance under high-temperature conditions and possess the excellent physical rigidity against the dendritic Li growth after long cycling test as well as provide the favorable Li ion permeability, which is also theoretically calculated by a density function theory (DFT) model. The high quality and nanosized h-BN sheets were fabricated by employing both the simple liquid and thermal expansion exfoliation method, which might give the great scalability and processability. The freestanding BNN separators (BNN-Ss) can successfully suppress the formation of protruding Li dendrites and possess the high thermal stability even at the high thermal conditions at ~120 ^{o}C, where the commercial polymer separators cannot handle those thermal conditions. In addition, the spinel lithium titanate (LTO) batteries with the freestanding BNN-Ss maintain a reversible coulombic efficiency of ~ 99% after the 600 cycles. These electrochemical and physical results imply the great potential of freestanding BNN-Ss as a key separator component for the future battery technology in stability and cyclability against internal and external surrounding environments.

Results and Discussion

The exfoliated *h*-BN nanosheets (BNNs) were prepared by using the combination of liquid exfoliation and thermal expansion techniques. The synthetic methods to yield the BNNs are schematically illustrated in **Fig. 1a** and **S1**. First, the bath and ultrasound probe sonification (liquid exfoliations) methods for *h*-BN bulk powders with a concentrated alkaline solution were carried out. These physical exfoliation methods can convert the bulk *h*-BN powders to the hydroxyl functionalized and small-sized thin *h*-BN layers. The hydrodynamic forces during the bath and ultrasound sonification can lead to the dramatic breakdown of the bulk BN powders into the thin BN layers. Simultaneously, the edge sites of the BN layers are simultaneously attacked by hydroxyl ions, and the hydroxyl ions are attached to the edge sites of thin *h*-BN as a functional group. Moreover, as shown in **Fig. S1**, during the gravimetric filtration process, the h-BN nanosheets can be stacked and laminated together with multiple layered structure. Moreover, during the lamination, the sheet-to-sheet van der Walls interactions become more effective. As shown in **Fig. S2**, X-ray photoelectron spectroscopy (XPS) spectra of both pristine BN powder and exfoliated BN have no difference. Especially, there are no split peaks and peak shift on the B1s and N1s of the both pristine BN powders and exfoliated BN layers, demonstrating the clear crystallinity of the exfoliated BN layers. Next, the secondary hydrogen (H_2)-assisted thermal expansion treatment was applied on the functionalized thin *h*-BN layers so as to further cleave the interlayers of the thin *h*-BN layers and to yield the nanosized BNNs. The finally obtained optimized BNNs were dispersed in an isopropyl alcohol (IPA) solution for the filtration process (**Fig. S3**). The freestanding BNN-Ss were further filtered by the vacuum filtration of the prepared exfoliated BNNs in the IPA solution. The vacuum filtration method enables the scalable fabrication of freestanding *h*-BN nanosheet-separators (BNN-Ss). Due to the fixed size of 2032-coin cells, the diameter and thickness of the freestanding BNN-Ss were carefully controlled by adjusting the amount and concentration of the BNN solution during filtration. The thickness of BNNs was about 20 ~ 30 μm, which is close to that of the commercial polymer separators.

It should be noted that the ion (H^+ and Li^+) permeability through the in- and out-plane of thin layer *h*-BN at the level of mono- and few-layers has been already demonstrated by other research groups [19,25,26]. The BNNs are successfully exfoliated into the mono- to few-layers of *h*-BN. Therefore, when the BNNs are further applied to the separator application, their thin in-plane structure can successfully provide the Li ion diffusion paths. **Fig. 1b** presents the morphologies and height profiles of the exfoliated BNN samples examined by atomic force microscopy (AFM). The thicknesses of representative BNNs were determined to be the mono- and bilayers, which are about 0.48 nm, and 0.90 nm, respectively [27]. **Fig. S4a** presents the Raman peak of bulk BN powders centered at near 1366 cm^{-1} (the E_{2g} mode (G band), B-N vertical vibrational mode within layers). Distinctly, the Raman peak of BNNs exhibits the relatively slight blue shift up to 4 cm^{-1}, which is a clear signature of the thin thickness of BNNs [28]. Note that the shift of the G band of *h*-BN is strongly correlated to its thickness: the thin thickness of *h*-BN presents an upshifted G band, while the thicker *h*-BN shows the downshift of the Raman peak position. **Fig. S4b** presents the Small-angle X-ray Scatting (SAXS) results of BNNs. The slope of the SAXS scattering intensity profile at very low q values is found to be 2.14, indicating the perfect dispersion of BNNs before the filtration process [29-30]. High-angle annular dark-field scanning transmission electron microscopy (HAADF-STEM) images of BNNs were also performed as shown in **Fig. 1c**. The inset TEM image of **Fig. 1c** represents the thin layers of BNNs. Moreover, the crystal images of BNNs include the well-organized honeycomb structure. The magnified HAADF-STEM image also clearly depicts the atomic structural characteristic of BNNs along with the distribution of B and N atoms. The hexagonal symmetric selective area electron diffraction (SAED) patterns in **Fig. 1d** imply that the BNNs are well matched with theoretical *h*-BN crystal structure [31]. Likewise, the STEM height line profiling of BNNs further indicates the existence of the N atoms and B atoms along with the in-plane direction of the BNN crystals. **Fig. S5** shows the TEM images of the exfoliated BNNs with few layered thicknesses. The most exfoliated BNNs have the diameters from few hundred nanometers to micrometers. These results indicate that the separator with the thin layers and small sizes of *h*-BN can guarantee the favorable ion diffusion paths through the in- or out-plane of BNNs. **Fig. 1e** depicts the freestanding BNN-Ss fabricated by the vacuum filtration method. The BNN-Ss can maintain its original structure even when it is strongly subjected to the different bending forces.

In order to evaluate and compare the heat-resistant properties of BNN-Ss and commercial polymer separators, thermal shrinkage tests were carried out at a temperature range from room temperature to 550 ºC. The visual images of BNN-Ss and commercial polymer separators after heat treatment at various temperatures are presented in the bottom and top of **Fig. 2a**, respectively. Shrinkage (%) is defined as the ratio of undamaged area to the area of an original separator and is also plotted as a function of increased temperature. The photo images clearly indicate that the commercial polymer separators started its volumetric degradation after the heat exposure about 80 ºC and lost over 70% of their original area upon the high temperature treatment (200 ºC), which is in good agreement with previously reported literatures [32-34]. On the other hand, the thermal shrinkage of BNN-Ss is negligibly small or not identified even up to 200 ºC. The more detailed shrinkage images of the commercial polymer separators and BNN-Ss are shown in **Fig. S6** and **S7**, respectively. Even at 550 ºC, the BNN-Ss well maintain its original round shape without any surface and volume degradation. These results indicate that the strong thermal durability of BNN-Ss can be strongly attributed to the superior intrinsic physical and chemical properties of *h*-BN. In addition, the wettability tests with an electrolyte solution and ionic conductivity tests were performed. Compared to the commercial polymer separators, the BNN-Ss exhibits the better wettability and electrolyte uptake, as shown in **Fig. 2b**, **2c** and **S8**. The variation of contact angles using droplets of the electrolyte solution was measured between the commercial polymer separators and the BNN-Ss. Specifically, the electrolyte uptake of BNN-Ss is found to be 256%, which is approximately 2 times higher than that of the commercial polymer separators. In addition, the ionic conductivity of BNN-Ss, evaluated by bulk resistance from electrochemical impedance spectroscopy (EIS) results (**Fig. S9)**, exhibits the reasonable value of 0.496 mS cm^{-1}, which is similar to that of the commercial polymer separators (0.461 mS cm^{-1}).

The distinct structural, thermal and ionic characteristics of *h*-BN properties and the as-prepared BN separators can be beneficial for the overall stability of Li ion cells during cycling. Especially, its extremely thermal stability can overcome any external thermal resources and the following malfunctions such as the deformation and decreased ionic conductivity of polymer separators. Also, the high rigidity of *h*-BN can handle all negative outcomes in cells by the natural growth of Li dendrites and the corresponding physical damage on polymer separators during cycling. To investigate the both iconic advantages of BNN-Ss from its physical and chemical properties, the BNN-Ss and commercial polymer separators were employed in the Li ion cells for the Li plating/stripping electrochemical experiment. It can be seen from **Fig. 3a** that a Cu plate (substrate), a Li foil and a 1.0 M $LiPF_6$ electrolyte were used as the working electrode, counter/reference electrode and electrolyte, respectively. The total Li plating capacity was set to be 1.0 mAh cm^{-2} on the Cu working electrode at a rate of 0.5 mA cm^{-2}. The Li stripping was then cycled to a cutoff potential of 2.0 V at the same rate of 0.5 mA cm^{-2}. Specifically, after 10 cycles, the electrochemical tests of the Li cells with the BNN-Ss and commercial polymer separators were paused and resumed after the 1hr thermal aging process in an oven to identify the experimental thermal stability of those separators. The coulombic efficiency was defined as the ratios between total Li plating and stripping capacity. As shown in **Fig. 3b**, before the aging process, the coulombic efficiencies (CE) on the Cu substrate during the Li plating/stripping are similar between the cells with the both separators. All cells can well maintain its initial CE values until first 10 cycles. After the aging process (the heat treatment while Li plating/stripping is stopped), the CE of the cells with the commercial polymer separators dropped to about 50% of its initial CE after 20 cycles. After aging at 80 ºC, the CE for commercial polymer separators is lowered due to the physical damage and shrinkage on the commercial separator. In contrast, the Li plating/stripping cells with the BNN-Ss can continuously guarantee its initial electrochemical properties, which are similar to the initial CE before the aging process. The dramatic CE differences right after the aging process can strongly represent that the high thermal stability of BNN-Ss might be essential to protect the stability of Li ion cells. Even in the severe conditions (after the aging process up to the 125 ºC, **Fig. S10**), the CE of the cells with BNN-Ss is close to ~ 80 % after 20 cycles. After aging at 125 ºC, the CE for the h-BN separators is well maintained, but slightly lowered. However, the CE for the commercial polymer separators is dramatically lowered due to the large physical damage and shrinkage on the commercial separator. It has been reported that the $LiPF_6$ electrolyte solution in organic carbonates is thermally stable up to 140 °C with non-electrochemical charge/discharge process [35]. Thus, these results are strongly attributed to the high thermal stability of *h*-BN while the degradation of commercial polymer separators occurs after thermal aging process.

The electrochemical behaviors of the Li plating/striping cells with the BNN-Ss and commercial polymer separators were further characterized by the over-potential (voltage) versus capacity (time) results after 1st cycle and 20nd cycle (including the aging process) (**Fig. 3c and 3d**, respectively). For the first Li plating/stripping cycle, the Li metal is deposited on the Cu foil during the Li plating, but some of the Li metal is left over on the Cu foil while the stripping processes (C.E. is not 100%). After a few cycles, the initial nucleation barrier on the Li/Cu foil is lower than that of the pristine Cu foil. The high nucleation density leads to a comparatively low plating overpotential. The Li plating/stripping over-potential of the cells with the BNN-Ss is slightly lower than that of the cells with the commercial polymer separators at 20th cycle. The Li stripping over-potentials of the commercial polymer separator and BNN-S is 312 mV and 129 mV at the time of 0.75 h, respectively. Over-potential values can indicate the status of Li plates on the Cu substrate which might result from the different structural and physical conditions of Li metal during cycling. The lower over-potentials of the cells with the BNN-Ss can representatively indicate the favorably deposited Li plates on the Cu substrate to continue the stable cycling performance of Li ion cells [22,24]. Moreover, there is a large voltage hysteresis (over-potential differences) at the cells with the commercial polymer separators, which is usually determined by the unfavorable interfacial charge-transfer properties. Those differences on the voltage versus capacity results might be strongly attributed to the morphologies of Li on the Cu substrate. The curve of the cells with the BNN-Ss after 20 cycles, after the aging process, indicates the longer capacitance (time) before reaching the cutoff potential of 2.0 V compared to the commercial polymer separators, subsequently demonstrating the CE with the BNN-Ss. The morphologies of the Li plates on the Cu substrate were visually investigated using scanning electron microscopy (SEM). The SEM images were taken after the heat treatment of 80 ºC after 10 cycles and then the electrochemical test was continued for additional 10 cycles. As shown in **Fig. 3f**, the Li plates on the Cu substrate with the commercial polymer separators present the typical protruding and dendritic Li metal, including many one-dimensional Li wires. Such protruding structures can cause the failure of separator component in LIB. Using the BNN-Ss, however, the resulting Li granules show the smooth and uniform formation on the Cu substrate **(Fig. 3e)**. The BNN-Ss show the high physical stability against the tensile strain from the Li dendrites after the electrochemical cycling. Due to the rigid and high physical stability of BNN-Ss, the cells with the BNN-Ss can physically inhibit protruding Li dendrite growth and successfully maintain its original electrochemical performance compared to the polymer-based separating materials as shown in schematically in **Fig. 3g** and **3h**. Collectively, the BNN-Ss can successfully provide the good thermal and physical stability of Li ion cells against the external and harsh heat environment as well as the physical deformation by the strain from dendritic Li growth. Therefore, in real LIB system, the BNN-Ss can decrease the risk of overall capacitance degradation and improve the cycling stability.

For the real application testing with the BNNS-s, as shown in **Fig. 4a**, the electrochemical performance of BNN-Ss with lithium titanate (LTO) and Li metal electrodes was further tested. The spinel LTO ($Li_4Ti_5O_{12}$) electrode has been used as the electrode because LTO possesses high power processability, a unique zero-strain effect, stable charge and discharge voltage (~1.6 V vs. Li/Li^+), and excellent cycling stability. The LTO electrodes were used due to its high rate capability and long cycle life. **Fig. 4b** presents a cyclic voltammetry of the LTO electrode with the BNN-Ss [36]. The LTO electrode exhibits a pair of sharp peaks at about 1.50 V and 1.65 V, which are characteristic of the Li insertion/extraction on LTO. The charge–discharge curves of BNN-Ss at a current density of 100 mA g^{-1} are shown in **Fig. 4c**. A pair of distinct and flat voltage plateau at around 1.50 V and 1.65 V reflects the well-known two-phase Li insertion/desertion equilibriums between $Li_4Ti_5O_{12}$ and $Li_7Ti_5O_{12}$ [37]. During the fist cycle, the plateau at around 1.5 V (vs. Li/Li+) would be related to the Li ion insertion/deintercalation of LTO and the small plateau at around 1.7 V (vs. Li/Li+) is induced by Li ion insertion/deintercalation of TiO_2 phase. During the initial insertion, the unexpected side insertion of Li ion into the TiO_2 dominant phase can make the following additional reduction plateau [38-41]. However, after the 1st cycle, the observed small plateau is negligible. The LTO with the BNN-Ss delivers an initial discharge capacity of 171.2 mAh g^{-1}. The LTO electrode with the BNN-Ss exhibits better long-term cycling stability than that of the commercial polymer separators even in the room temperature (**Fig. S11**). As shown in **Fig. 4d**, the LTO electrode with the BNN-Ss present a high coulombic efficiency of ~ 99 % up to 600 cycles, whereas that of the commercial polymer separators drops to ~ 78 %. **Fig. 4e** presents the rate-capability test of BNN-Ss and commercial polymer separators. At a current density of 1500 mA g^{-1}, the retention of the charge storage capacities of the LTO electrode with the BNN-Ss can reach a higher value of ~ 60% than that of the commercial polymer separators. These results might be attributed to the high wettability and ionic conductivity of BNN-S and further suggest that the BNN-Ss play a pivotal role for the enhanced energy storing kinetics and stable operation/cyclability of LIBs (Table S1). Due to the thickness difference, the ionic conductivity of BNN-Ss, calculated using R_b and thickness of separator, shows the value of 0.496 mS cm^{-1}, which is slightly higher than or comparable to that of the commercial polymer separators (0.461 mS cm^{-1}). Moreover, the contact angle and electrolyte uptake results obtaining from the droplets of the electrolyte solution on the separators samples represent the high interface interaction between the solution and BNN-S as shown in Figure 2b and 2c. As illustrated in **Fig. 4f** and **4g**, similar to previous results,[21,22,24] the commercial polymer separators are not proper candidates to block the piercing Li dendrites growth on the Li metal electrode. In contrast, the uniform and smooth deposition of the additional Li dendrites by the BNN-Ss with superior thermal and physical stabilities can induce the better cyclability than the commercial polymer separators. The possible diffusion mechanism of Li ions through BNN-Ss might be attributed to the mitigation through atomic defects which are formed during the exfoliation steps. The feasibility of those defects working as the potential ion diffusion paths is demonstrated by density-functional theory (DFT) calculations (**Fig. S12**). **Fig. S12d** also shows the auxiliary DFT calculations for input models obeying the exact charge neutrality. On the exfoliated *h*-BN sheets, there can be two possible atomic defects which are placed in the location where the nitrogen or borone atomic bonding is broken. Based on the activation barrier energy calcualtion, the diffusion paths thorugh those two defects show the lower activation barrier energy of Li electrolyte ions compared to the pristine BN structure.

Conclusion

In summary, new synthetic methods of thin *h*-BN nanosheets are developed and have successfully resulted in the *h*-BN nanosheets as the freestanding separators for electrochemical energy storage applications. The resultant freestanding *h*-BN nanosheet separators exhibit the excellent physical rigidity during the cycling and thermal endurance against the high-temperature environments without the dramatic performance degradation as well as show the good Li ion diffusion kinetics. The *h*-BN separators can handle ~ 120 °C external heat without the structural collapse and also well maintain its initial coulombic efficiency during the Li deposition on the Cu substrate. The free-standing *h*-BN separators can maintain a reversible coulombic efficiency of ~ 99% after the 600 cycles with the LTO electrodes. The strong thermal and physical durability of the freestanding *h*-BN nanosheet separators can be strongly correlated to the superior intrinsic physical and chemical feasibility of *h*-BN. Moreover, the density functional theory (DFT) calculation reveals that the small defect sites on the *h*-BN nanosheets can induce the much favorable Li ion penetration along with the sheets and corresponding separators. Thus, based upon these findings, the facile and efficient processability of the *h*-BN nanosheets and the corresponding freestanding separators can further extend the applicability of energy storage applications in near future.

ASSOCIATED CONTENT

- Supporting Information

Experimental methods, Schematic illustration of the exfoliation process, XPS spectra before and after exfoliation method, Real image of exfoliated h-BN nanosheets, Raman spectra of pristine h-BN powder and exfoliated h-BN, SAXS analysis of BNNs, TEM images, Thermal stability tests of commercial separators and BNN-S, Electrolyte wettability test, Impedance plots, Coulombic efficiency (CE) versus cycle plots after 125 °C thermal aging step, Capacity cycling retention of LTO//Li cells, DFT crystal models of h-BN defects, Parameters for ionic conductivity calculation.

- Author Information

Corresponding Authors

E-mail: ywlee@sch.ac.kr

E-mail: junginn.sohn@dongguk.edu

- Author Contributions

J.H and A.-R.J. equally contributed to this work. J.H, A.-R.J., Y.-W.L. and J.I.S. conceived the idea. J.H, A.-R.J., and Y.-W.L. synthesized the samples, analyzed the data, and wrote the manuscript; W.B.P. and K.-S.S. analyzed the DFT data. B.H. analyzed the TEM data. K.-S.S., J.-O. L. S.N.C., Y.-W.L, J.I.S. contributed in reviewing the manuscript and provided scientific input.

- Notes

The authors declare no competing financial interest

- Acknowledgements

This research was supported by the National Research Foundation of Korea grant funded by the Korea government (MSIT) (2019R1F1A1041407, 2019M1A2A2065616, 2019R1A4A1021237, and 2019R1A2C1007883) and by the Soonchunhyang University Research Fund.

References

[1] Tarascon, J.-M.; Armand, M. Issues and challenges facing rechargeable lithium batteries. *Nature* **2001**, *414*, 359-367.

[2] Li, M.; Lu, J.; Chen, Z.; Amine, K. 30 Years of lithium-ion batteries. *Adv. Mater.* **2018**, *30*, 1800561.

[3] Wang, K.-X.; Li, X.-H.; Chen, J.-S. Surface and interface engineering of electrode materials for lithium-ion batteries. *Adv. Mater.* **2015**, *27*, 527-545.

[4] Liu, J.; Bao, Z.; Cui, Y.; Dufek, E.; Goodenough, J.; Khalifah, P.; Li, Q.; Liaw, B. Y.; Liu, P.; Manthiram, A.; Meng, S.; Subramanian, V.; Toney, M.; Viswanathan, V.; Whittingham, S.; Xiao, J.; Xu, W.; Yang, J.; Yang, X.-Q.; Zhang, J.-G. Pathways for practical high-energy long-cycling lithium metal batteries. *Nat. Energy* **2019**, *4*, 180-186.

[5] Nitta, N.; Wu, F.; Lee, J.; Yushin, G. Li-ion battery materials: present and future. *Mater. Today* **2015**, *18*, 252-264.

[6] Alias, N.; Mohamad, A. Advances of aqueous rechargeable lithium-ion battery: A review. *J. Power Sources* **2015**, *274*, 237-251.

[7] Lee, H.; Yanilmaz, M.; Toprakci, O.; Fu, K.; Zhang, X. A review of recent developments in membrane separators for rechargeable lithium-ion batteries. *Energy Environ. Sci.* **2014**, *7*, 3857-3886.

[8] Lee, Y.-W.; An, G.-H.; Kim, B.-S.; Hong, J.; Pak, S.; Lee, E.-H.; Cho, Y.; Lee, J.; Giraud, P.; Cha, S.; Ahn, H.-J.; Sohn, J.; Kim, J. Synergistic effects of a multifunctional graphene based interlayer on electrochemical behavior and structural stability. *ACS Appl. Mater. Inter.* **2016**, *8*, 17651-17658.

[9] Gauthier, M.; Carney, T.; Grimaud, A.; Giordano, L.; Pour, N.; Chang, H.-H.; Fenning, D.; Lux, S.; Paschos, O.; Bauer, C.; Maglia, F.; Lupart, S.; Lamp, P.; Shao-Horn, Y. Electrode–electrolyte interface in Li-Ion batteries: current understanding and new insights. *J. Phys. Chem. Lett.* **2015**, *6*, 4653-4672.

[10] Li, L.; Li, S.; Lu, Y. Suppression of dendritic lithium growth in lithium metal-based batteries. *Chem. Commun.* **2018**, *54*, 6648-6661.

[11] Cheng, X.-B.; Zhang, R.; Zhao, C.-Z.; Zhang, Q. Toward safe lithium metal anode in rechargeable batteries: A review. *Chem. Rev.* **2017**, *117*, 10403-10473.

[12] Woo, J.-J.; Zhang, Z.; Rago, N.; Lu, W.; Amine, K. A high performance separator with improved thermal stability for Li-ion batteries. *J. Mater. Chem. A* **2013**, *1*, 8538-8540.

[13] Liu, B.; Zhang, J.-G.; Xu, W. Advancing lithium metal batteries. *Joule* **2018,** *2*, 833-845.

[14] Xu, W.; Wang, J.; Ding, F.; Chen, X.; Nasybulin, E.; Zhang, Y.; Zhang, J.-G. Lithium metal anodes for rechargeable batteries. *Energy Environ. Sci.* **2014**, *7*, 513-537.

[15] Yang, Y.; Wang, W.; Li, L.; Li, B.; Zhang, J. Stable cycling of Li–S batteries by simultaneously suppressing Li-dendrite growth and polysulfide shuttling enabled by a bioinspired separator. *J. Mater. Chem. A* **2020**, *8*, 3692-3700.

[16] Yang, J.; Wang, C.-Y.; Wang, C.-C.; Chen, K.-H.; Mou, C.-Y.; Wu, H.-L. Advanced nanoporous separators for stable lithium metal electrodeposition at ultra-high current densities in liquid electrolytes. *J. Mater. Chem. A* **2020**, *8*, 5095-5104.

[17] Wu, X.; Liu, N.; Guo, Z.; Wang, M.; Qiu, Y.; Tian, Y.; Tian, D.; Guan, B.; Fan, L.; Zhang, N. Constructing multi-functional Janus separator toward highly stable lithium batteries. *Energy Storage Mater.* **2020**, *28*, 153-159.

[18] Zhang, K.; Feng, Y.; Wang, F.; Yang, Z.; Wang, J. Two dimensional hexagonal boron nitride (2D-hBN): synthesis, properties and applications. *J. Mater. Chem. C* **2017**, *5*, 11992-12022.

[19] Hu, S. Lozada-Hidalgo, M.; Wang, F. C.; Mishchenko, A.; Schedin, F.; Nair, R. R.; Hill, E. W.; Boukhvalov, D. W.; Katsnelson, M. I.; Dryfe, R. A. W.; Grigorieva, I. V.; Wu, H. A.; Geim, A. K. Proton transport through one-atom-thick crystals. *Nature* **2014**, *516*, 227-230.

[20] Mortazavi, B.; Yang, H.; Mohebbi, F.; Cuniberti, G.; Rabczuk, T. Graphene or h-BN paraffin composite structures for the thermal management of Li-ion batteries: A multiscale investigation. *Appl. Energy* **2017**, *202*, 323-334.

[21] Yan, K.; Lee, H.-W.; Gao, T.; Zheng, G.; Yao, H.; Wang, H.; Lu, Z.; Zhou, Y.; Liang, Z.; Liu, Z.; Chu, S.; Cui, Y. Ultrathin two-dimensional atomic crystals as stable interfacial layer for improvement of lithium metal anode. *Nano Lett.* **2014**, *14*, 6016-6022.

[22] Xie, J.; Liao, L.; Gong, Y.; Li, Y.; Shi, F.; Pei, A.; Sun, J.; Zhang, R.; Kong, B.; Subbaraman, R.; Christensen, J.; Cui, Y. Stitching h-BN by atomic layer deposition of LiF as a stable interface for lithium metal anode. *Sci. Adv.* **2017**, *3*, eaao3170

[23] Kim, P. J. H.; Seo, J.; Fu, K.; Choi, J.; Liu, Z.; Kwon, J.; Hu, L.; Paik, U. Synergistic protective effect of a BN-carbon separator for highly stable lithium sulfur batteries. *NPG Asia Mater.* **2017**, *9*, e375.

[24] Luo, W.; Zhou, L.; Fu, K.; Yang, Z.; Wan, J.; Manno, M.; Yao, Y.; Zhu, H.; Yang, B.; Hu, L. A thermally conductive separator for stable Li metal anodes. *Nano Lett.* **2015**, *15*, 6149-6154.

[25] Kroes, J. M. H.; Fasolino, A.; Katsnelson, M. I. Density functional based simulations of proton permeation of graphene and hexagonal boron nitride. *Phys. Chem. Chem. Phys.* **2017,** *19*, 5813-5817.

[26] Tian, H.; Seh, Z. W.; Yan, K.; Fu, Z.; Tang, P.; Lu, Y.; Zhang, R.; Legut, D.; Cui, Y.; Zhang, Q. Theoretical investigation of 2D layered materials as protective films for lithium and sodium metal anodes. *Adv. Funct. Mater.* **2017**, *7,* 1602528.

[27] Falin, A.; Cai, Q.; Santos, E.; Scullion, D.; Qian, D.; Zhang, R.; Yang, Z.; Huang, S.; Watanabe, K.; Taniguchi, T.; Barnett, M.; Chen, Y.; Ruoff, R.; Li, L. H. Mechanical properties of atomically thin boron nitride and the role of interlayer interactions. *Nat. Commun.* **2017**, *8*, 15815.

[28] Li, L. H.; Chen, Y. Atomically thin boron nitride: unique properties and applications. *Adv. Funct. Mater.* **2016**, *26*, 2594-2608.

[29] Hoda, N.; Antoni, S.-F.; Jozef, A.; Stephan H.; Hossein, M.; Nader, Q.; Raffaele, M. Gelatin–Graphene Nanocomposites with Ultralow Electrical Percolation Threshold. *Adv. Mat.* **2016**, *28*, 6914-6920.

[30] Thomas, M.; Liliana, C.; Anna, S.; Isabelle, G.; Ekaterina, I.; Rico, T. Bulk properties of aqueous graphene oxide and reduced graphene oxide with surfactants and polymers: adsorption and stability. *Phys. Chem. Chem. Phys.* **2018**, *20*, 16801-16816.

[31] Oh, H.; Jo. J.; Tchoe, Y.; Yoon, H.; Lee, H. H.; Kim, S.-S.; Kim, M.; Sohn, B.-H.; Yi, G.-C. Centimeter-sized epitaxial h-BN films. *NPG Asia Mater.* **2016**, *8*, e330.

[32] Wu, D.; Shi, C.; Huang, S.; Qiu, X.; Wang, H.; Zhan, Z.; Zhang, P.; Zhao, J.; Sun, D.; Lin, L. Electrospun nanofibers for sandwiched polyimide/poly (vinylidene fluoride)/polyimide separators with the thermal shutdown function. *Electrochim. Acta* **2015**, *176,* 727-734.

[33] Liao, H.; Zhang, H.; Qin, G.; Li, Z.; Li, L.; Hong, H. A macro-porous graphene oxide-based membrane as a separator with enhanced thermal stability for high-safety lithium-ion batteries. *RSC Adv.* **2017**, *7,* 22112-22120.

[34] Blake, A. J.; Kohlmeyer, R. R.; Hardin, J. O.; Carmona, E. A.; Maruyama, B.; Berrigan, J. D.; Huang, H.; Durstock, M. F. 3D printable ceramic–polymer electrolytes for flexible high-performance Li-ion batteries with enhanced thermal stability. *Adv. Energy Mater.* **2017**, *7*, 1602920.

[35] Gnanaraj, J. S.; Zinigrad, E.; Asraf, L.; Gottlieb, H. E.; Sprecher, M.; Schmidt, M.; Geissler, W.; Aurbach, D. A. detailed investigation of the thermal reactions of $LiPF_6$ solution in organic carbonates using ARC and DSC. *J. Electrochem. Soc*. **2003**, *150*, A1533-A1537.

[36] Krajewski, M.; Hamankiewicz, B.; *Michalska*, M.; Andrzejczuk, M.; Lipinska, L.; Czerwinski, A. Electrochemical properties of lithium–titanium oxide, modified with Ag–

Cu particles, as a negative electrode for lithium-ion batteries. *RSC Adv.* **2017**, *7*, 52151-52164.

[37] Chen, C.; Agrawal, R.; Wang, C. High performance $Li_4Ti_5O_{12}$/Si composite anodes for Li-ion batteries. *Nanomaterials* **2015**, *5*, 1469-1480.

[38] Lou, S.; Zhao, Y.; Wang, J.; Yin, G.; Du, C.; Sun, X. Ti-based oxide anode materials for advanced electrochemical energy storage: Lithium/sodium ion batteries and hybrid pseudocapacitors. *Small* **2019**, *15*, 1904740

[39] Gangaja, B.; Nair, S. V.; Santhanagopalan, S. nterface-engineered $Li_4Ti_5O_{12}$–TiO_2 dual-phase nanoparticles and CNT additive for supercapacitor-like high-power Li-ion battery applications. *Nanotechnol.* **2018**, *29*, 095402.

[40] Liao, J.-Y.; Chabot, V.; Gu, M.; Wang, C.; Xiao, X.; Chen, Z. Dual phase $Li_4Ti_5O_{12}$-TiO_2 nanowire arrays as integrated anodes for high-rate lithium-ion batteries. *Nano Energy* **2014**, *9*, 383-391.

[41] Lukman, N.; Rais, F.; Haniffudin, N.; Hariyati, P.; Achmand, S.; Joko, T.; Bambang P. Synthesis of dual-phase $Li_4Ti_5O_{12}$-TiO_2 nanowires as anode for lithium-ion battery. *Ionics* **2019**, *25*, 1505-1511.

Figure Captions

Figure 1. (a) A schematic image of exfoliated *h*-BN nanosheets. (b) AFM images of mono- and bi-layer BNNs & Linear AFM depth profiles of mono- and bi-layer BNNs. (c) A HAADF-STEM image of BNNs. The inset image shows a TEM image of BNNs. (d) A high resolution STEM image, SAED pattern and atomic line profile of BNNs. (e) Optical images of BNN-Ss.

Figure 2. (a) Thermal deformation tests of BNN-Ss and commercial polymer separators up to 300 °C (b) Contact angle (CA) of BNN-Ss and commercial separators with electrolyte solvents. (c) Electrolyte uptake (EU) calculation of BNN-Ss and commercial separators.

Figure 3. A schematic illustration of (a) Li plating/stripping experiment cells with BNN-Ss and commercial polymer separators. (b) Coulombic efficiency (CE) versus cycle plots with BNN-Ss and commercial polymer separators after 80 °C thermal aging process. Potential versus time plots during Li plating/stripping cycling with (c) BNN-Ss and (d) commercial polymer separators. SEM characterization of Li plating on the Cu substrate with (e) BNN-Ss and (f) commercial polymer separators. Schematic illustrations of deposited Li dendrites with (g) BNN-Ss (flat structures) and (h) commercial polymer (protruding structures).

Figure 4. (a) A schematic ion diffusion illustration of LTO//Li cells with BNN-Ss. (b) Cyclic voltammetry of LTO//Li cells. (c) Charge-discharge curves of LTO//Li cells with BNN-Ss. (d) Coulombic efficiency of LTO//Li cells with BNN-Ss and commercial polymer separators. (e) Capacity rate retention of LTO//Li cells with BNN-Ss and commercial polymer separators. Schematic characterization of cycled Li metal electrodes in LTO//Li cells with (f) BNN-Ss and (g) commercial polymer separators.

Fig. 1. J. Hong et al.

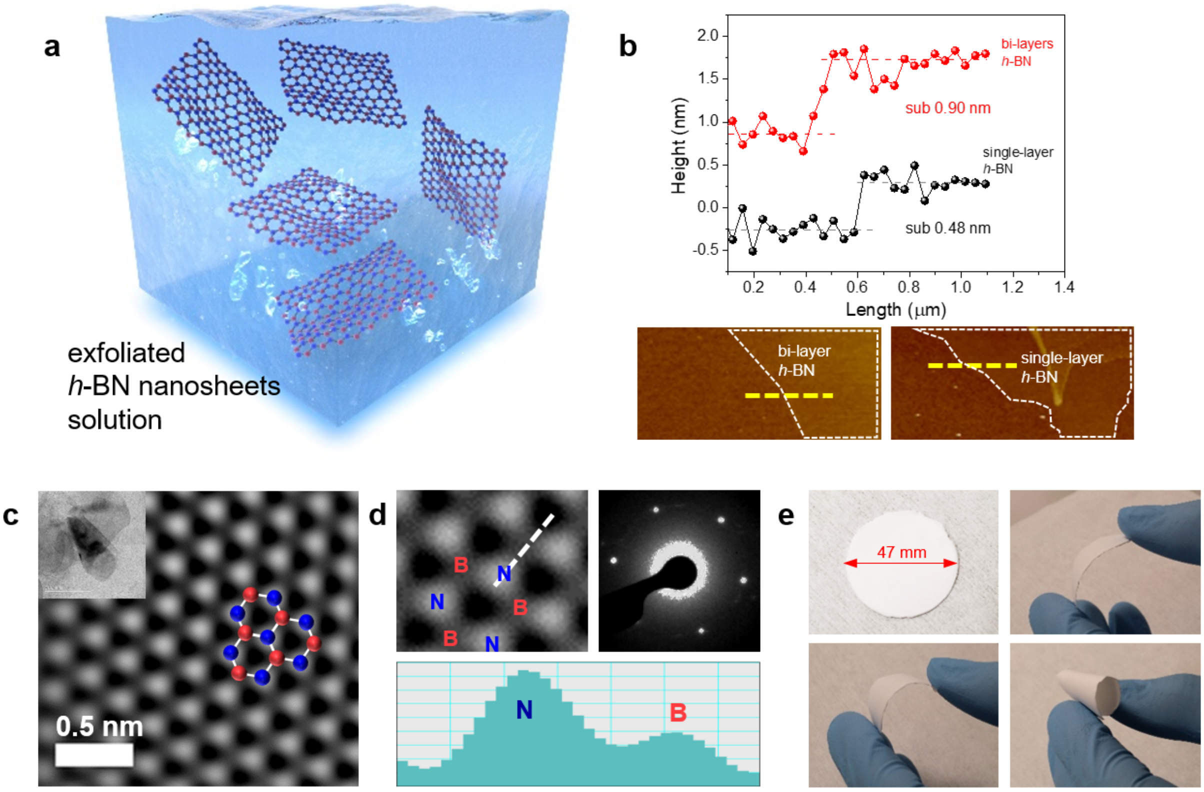

Fig. 2. J. Hong et al.

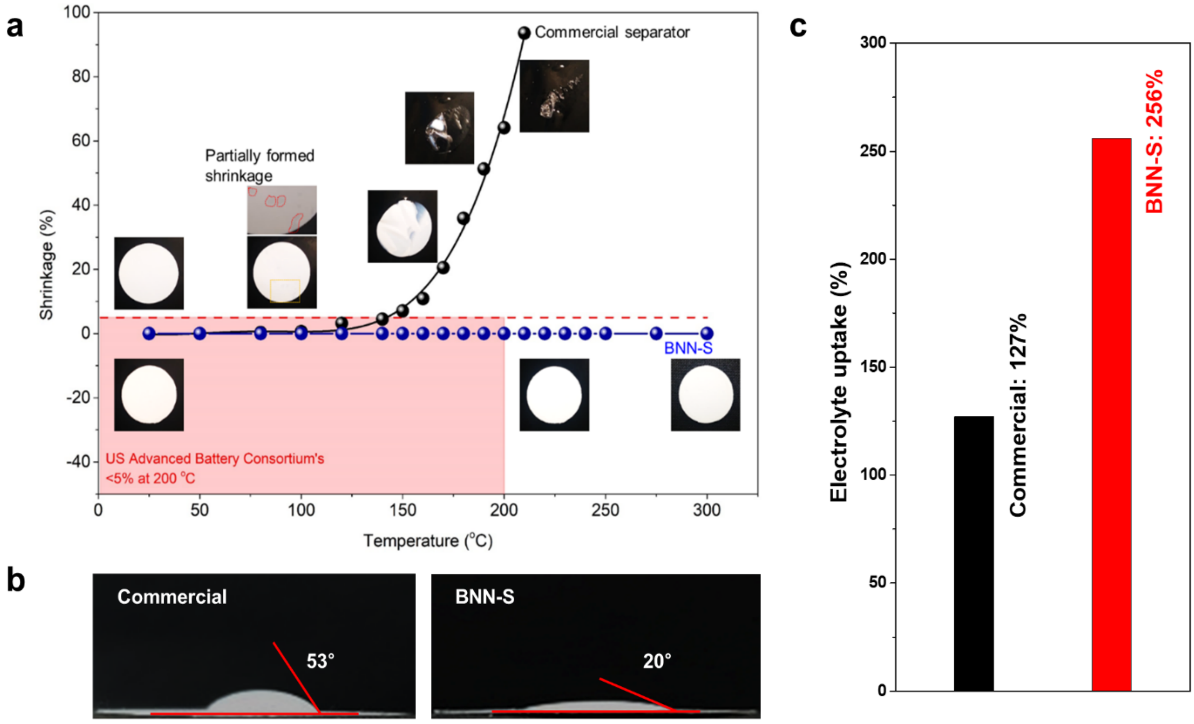

Fig. 3. J. Hong et al.

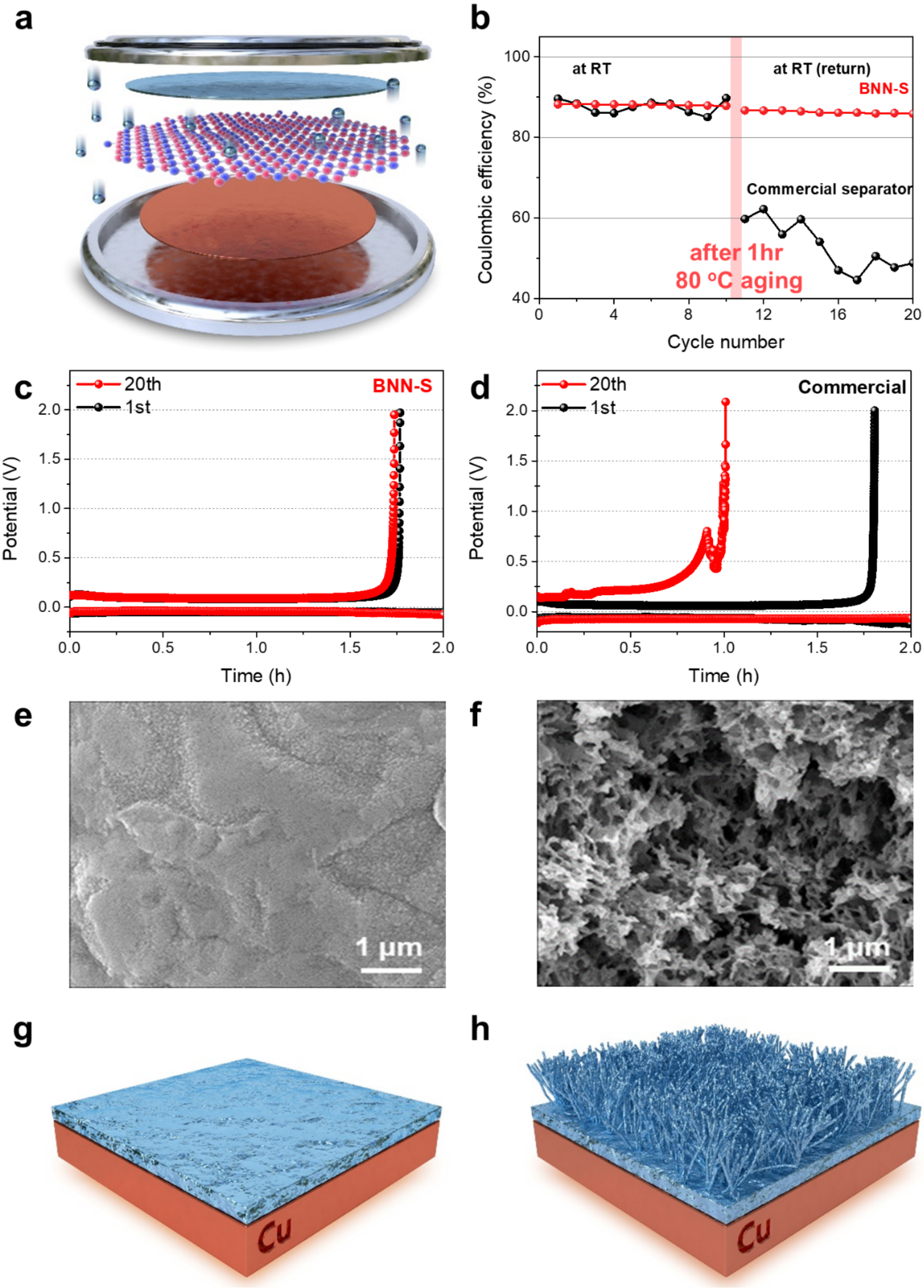

Fig. 4. J. Hong et al.

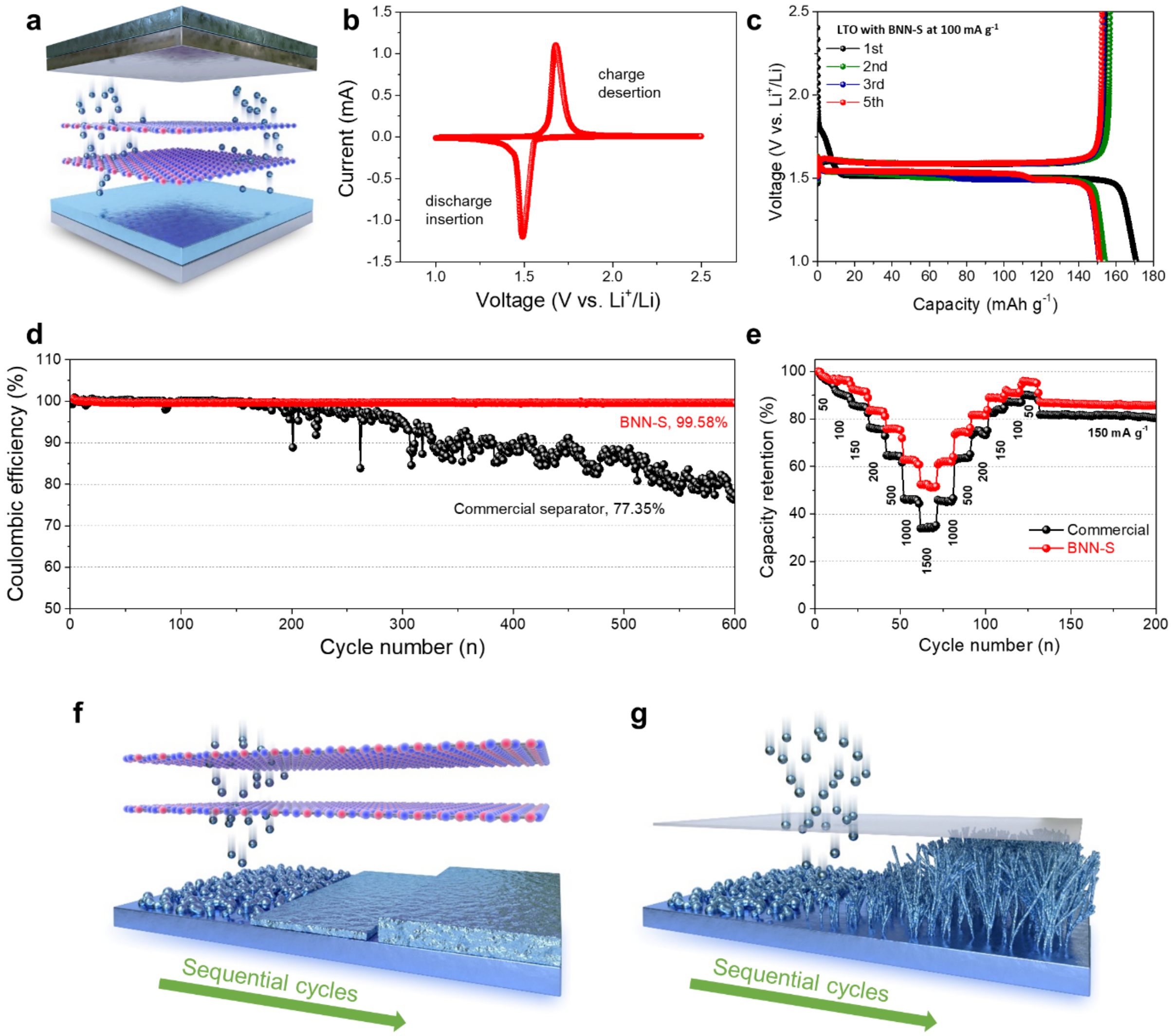

For Table of Contents Use Only

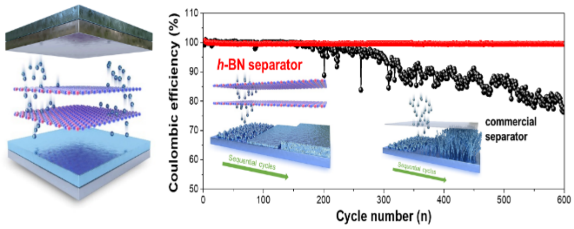

Freestanding *h*-BN nanosheet separator show the high electrochemical performance in Li ion battery including high physical and thermal stability.